NASA Technical Memorandum 81914

Effects of Angle of Attack and ~~Ventra~~ VERTICAL Fin on Transonic Flutter Characteristics of an Arrow-Wing Configuration

Robert V. Doggett, Jr., and Rodney H. Ricketts

DECEMBER 1980

NASA

errata changes made 3-6-81

ERRATA

NASA Technical Memorandum 81914

EFFECTS OF ANGLE OF ATTACK AND VENTRAL FIN ON TRANSONIC FLUTTER CHARACTERISTICS OF AN ARROW-WING CONFIGURATION

December 1980

Robert V. Doggett, Jr., and Rodney H. Ricketts

The word "ventral" was inadvertently used for "vertical" to describe the fin in this report. The word "ventral" should be changed to "vertical" in the following places:

Cover page, second line of title

Title page, second line of title

Page 1, line 4 and last line

Page 3, first paragraph, lines 5 and 7

Page 8, line 5 of CONCLUSIONS

Last page (Report Documentation Page), first line of title and third line of abstract

Also,

Page 12: Change "Basic-Wing" to "Wing-With-Fin" in title of table II

Last page (Report Documentation Page): In Block 18, change Subject Category to 39.

ISSUE DATE:

March 5, 1981

NASA Technical Memorandum 81914

Effects of Angle of Attack and ~~Ventral~~ Vertical Fin on Transonic Flutter Characteristics of an Arrow-Wing Configuration

Robert V. Doggett, Jr., and Rodney H. Ricketts
Langley Research Center
Hampton, Virginia

National Aeronautics
and Space Administration

**Scientific and Technical
Information Branch**

1980

SUMMARY

Experimental transonic flutter results are presented for a simplified 1/50-size, aspect-ratio-1.77 wind-tunnel model of an arrow-wing design. Flutter results are presented for two configurations; namely, one with and one without a ~~ventral~~ vertical fin mounted at the 0.694 semispan station. Results are presented for both configurations trimmed to zero lift and in a lifting condition at angles of attack up to 4°. The results show that the flutter characteristics of both configurations are similar to those usually observed. Increasing angle of attack reduces the flutter dynamic pressure by a small amount (about 13 percent maximum) for both configurations. The addition of the fin to the basic wing increases the flutter dynamic pressure. Calculated results for both configurations in the nonlifting condition obtained by using subsonic doublet-lattice unsteady aerodynamic theory correlate reasonably well with the experimental results. Calculated results for the basic wing obtained by using subsonic kernel-function unsteady aerodynamic theory did not agree as well with the experimental data.

INTRODUCTION

Because supersonic-cruise transport airplane configurations of interest in the United States are large and flexible, a strength-design structure often does not have sufficient stiffness to satisfy flutter margin requirements. Several design studies have been made in sufficient detail to indicate that the flutter deficiency may be rather large for supersonic-cruise transports. Early arrow-wing configurations (refs. 1 and 2) required the addition of over 4536 kg (10 000 lbm) of structural mass to the strength design to increase flutter speeds to an acceptable level. Other studies of arrow-wing designs (refs. 3 and 4) have shown a smaller, but nonetheless substantial, mass penalty. There is, consequently, considerable interest in understanding better the flutter characteristics of candidate supersonic-cruise transport airplane configurations. A low-aspect-ratio arrow wing was chosen for the present study because the NASA-sponsored supersonic cruise research (SCR) program has focused on this type of configuration.

Experimental transonic flutter boundaries are presented for an aspect-ratio-1.77, semispan, cantilever-mounted wind-tunnel model having an arrow-wing planform with a 3-percent-thick elliptical biconvex airfoil section. Essentially this same wing model was used in a previous investigation (ref. 5) which addressed basic arrow-wing flutter characteristics and the effects of engine nacelle geometry on flutter. Although this model wing is not a dynamically scaled aeroelastic model of a particular full-scale wing, it is a simplified 1/50-size representation of arrow-wing configurations of current interest. The experiments were conducted in the Langley Transonic Dynamics Tunnel. Experimental flutter results are presented for the basic wing in a nonlifting condition (angle of attack $\alpha = 0°$) and in lifting conditions ($\alpha = 2°$, $3°$, and $4°$). In addition, flutter results are presented for the basic wing with a ~~ventral~~ vertical fin

errata
3-6-81

which was located at the 0.694 semispan station. The effects of lift also were studied using the wing-with-fin configuration, and data are presented for angles of attack of 0° and 4°. The experimental results for the nonlifting case for both configurations are correlated with calculated results obtained by using subsonic doublet-lattice unsteady aerodynamic theory. Calculated results for the basic-wing configuration obtained by using subsonic kernel function unsteady aerodynamic theory are presented also.

Use of trademarks in this report does not constitute an official endorsement, either expressed or implied, by the National Aeronautics and Space Administration.

SYMBOLS

Measurements and calculations were made in the U.S. Customary Units and are presented in both the International System of Units (SI) and U.S. Customary Units.

b_r reference semichord, m(ft)

f frequency, Hz

f_f flutter frequency, Hz

f_2 measured frequency of second natural mode, Hz

M Mach number

m mass, kg (lbm)

q dynamic pressure, $1/2\ \rho V^2$, Pa (lbf/ft^2)

V velocity, m/sec (ft/sec)

V_I flutter-speed index parameter, $\frac{V}{b_r \omega_2 \sqrt{\mu}}$

v reference volume, m^3 (ft^3)

α angle of attack measured from zero lift, deg

μ mass ratio parameter, $\frac{m}{\rho v}$

ρ density, kg/m^3 ($slug/ft^3$)

ω_2 reference circular frequency, $2\pi f_2$, rad/sec

Subscripts:

c calculated

m measured

MODELS

The basic wing model had an arrow-wing planform with panel aspect ratio of 1.77. Although this model wing is not a dynamically scaled aeroelastic model of a particular full-scale airplane, it is a 1/50-size simplified representation of arrow-wing designs of current interest. A second model configuration consisting of the basic wing with a ~~ventral~~ vertical fin attached at 0.694 semispan station was used also. The mass of the wing was 6.68 kg (3.03 lbm); the mass of the ~~ventral~~ vertical fin was 0.035 kg (0.0772 lbm). Geometric details of the models are given in figure 1. Photographs showing the wing-with-fin model mounted in the wind tunnel are shown in figure 2. (The engine nacelles shown mounted on the lower surface in the photograph were not used in the present study. See ref. 5.)

Construction

The wing was constructed of a 0.2286-cm-thick (0.090-in.) aluminum-alloy plate that was beveled to a sharp edge along the leading and trailing edges. The plate was covered with balsa wood to give the desired 3-percent-thick elliptical biconvex airfoil section. To minimize the effects of the balsa wood on the wing stiffness, the grain of the wood was orientated perpendicular to the plate. The plate was extended inboard of the wing root to provide a base for clamping the model in a cantilever fashion. Saw cuts (fig. 1) were made in the plate at both the leading and trailing edges along the wing root so that the model was cantilever mounted along 81 percent of the root chord. This mounting arrangement provided an approximate simulation of the wing-fuselage attachment of a full-size arrow wing.

The fin was made from 0.127-cm-thick (0.050-in.) aluminum-alloy plate. The leading edge of the fin was beveled to a sharp edge. The fin was attached to the wing by small machine screws that passed through four tabs located at the base of the fin. These tabs, which were formed from the same piece of aluminum plate, were integral parts of the fin structure. (See fig. 1.) The balsa wood was removed from the wing at the attachment points so that the tabs mounted directly to the wing plate.

Vibration Characteristics

The first six natural frequencies and node lines were measured for the basic-wing configuration; the first seven natural frequencies and node lines were measured for the wing-with-fin configuration. The first six frequencies and node lines for both configurations are presented in figure 3. Calculated

results obtained by using the NASA Structural Analysis (NASTRAN[1]) computer program are shown in the figure also. NASTRAN is described in detail in references 6 and 7. In the analysis, the structure was represented by a combination of triangular (NASTRAN TRIA2) and quadrilateral (NASTRAN QUAD2) structural elements arranged as shown in figure 4. The mass and stiffness of both the balsa wood and aluminum plate were accounted for in the finite element model.

In general, the agreement between the measured and calculated natural frequencies and node lines is good. A comparison of the basic-wing data (fig. 3(a)) with the wing-with-fin data (fig. 3(b)) shows that the first three modes are very similar. The addition of the fin to the wing has little effect on these node lines or frequencies. The node lines for the fourth basic-wing mode are somewhat similar to the fourth and fifth wing-with-fin node lines, especially with respect to the measured ones. The fifth basic-wing mode and the sixth wing-with-fin mode appear to be the same type of mode. The sixth basic-wing mode is similar to the seventh wing-with-fin mode (not shown in the figure, f_m = 158.6 Hz, f_c = 175.0 Hz). The primary effect of adding the fin to the wing was the introduction of an additional mode between the fourth and fifth basic-wing modes. It was observed during the ground vibration tests that the most elastic deformation of the fin relative to wing deformation occurred for the fifth wing-with-fin mode.

FLUTTER EXPERIMENTS

Wind Tunnel

The flutter experiments were conducted in Freon[2] 12 in the Langley Transonic Dynamics Tunnel. This facility is a slotted-throat single-return wind tunnel that has a 4.88-m (16-ft) square test section with cropped corners. The stagnation pressure can be varied from slightly above atmospheric to near vacuum; the Mach number can be varied over the range from 0 to 1.2. The tunnel is of the continuous-operation type and is powered by a motor-driven fan. Both test section Mach number and density are continuously controllable. The tunnel is equipped with four quick-opening bypass valves that are used when flutter occurs to rapidly reduce the test-section dynamic pressure and Mach number.

Test Procedure

The wing was cantilever mounted from a splitter plate that was mounted 15.24 cm (6 in.) off the tunnel wall on a bracket. This bracket was attached to a remotely controlled turntable which was used to change the model angle of

---

[1]NASTRAN: Registered trademark of the National Aeronautics and Space Administration.

[2]Freon: Registered trademark of E.I. du Pont de Nemours & Co., Inc.

attack. This mounting arrangement insured that the model root was outside the wind-tunnel-wall boundary layer. A portion of the splitter plate can be seen in figure 2.

Flutter boundaries were determined for the basic-wing and wing-with-fin configurations with the models positioned to zero lift ($\alpha = 0^{\circ}$). Additional flutter data were obtained for the basic wing at angles of attack of 2°, 3°, and 4°, and for the wing-with-fin at 4° angle of attack.

The same general procedure was used for all tests. A typical flutter boundary was determined as follows: With the wind tunnel evacuated to a low stagnation pressure, the tunnel fan speed was increased until the desired test-section Mach number was reached. With the Mach number held constant, the test section density was increased gradually until flutter occurred. At flutter onset, the test-section dynamic pressure and Mach number were decreased rapidly by opening the bypass valves. The fan speed was then decreased to a point well below the flutter condition and the bypass valves were closed. Next, angle-of-attack was increased, after which the test-section Mach number was slowly increased until flutter was experienced again. This same procedure was repeated several times to obtain enough flutter points to define the flutter boundary over the Mach number range of interest.

During each flutter test the output signals from resistance-wire strain-gage bridges mounted near the wing root were recorded on an oscillograph recorder. The flutter frequencies were determined from these oscillograph records. The natural frequencies of the model were obtained before and after each wind-tunnel test to determine whether or not the model had been damaged. No damage was detected throughout the test program.

FLUTTER ANALYSIS

Flutter calculations were made at Mach numbers 0.7, 0.8, and 0.9 for the basic-wing and wing-with-fin configurations by using the flutter analysis capability that has been incorporated into NASTRAN. The NASTRAN flutter analysis method is of the modal type and provides the user with various options in affecting the solution. See reference 8 for a description of the NASTRAN capability. The present results were obtained by using doublet lattice unsteady aerodynamic theory, surface splines to interpolate from structural to aerodynamic degrees of freedom, k-method for solving the flutter equation, and the first six calculated mode shapes and generalized masses. Measured natural frequencies were used in place of the calculated natural frequencies. The aerodynamic model for the wing consisted of 108 doublet-lattice boxes arranged 9 per chord at 12 spanwise stations. The aerodynamic model for the fin consisted of 60 boxes, 10 per chord at 6 spanwise stations. The corners of the boxes on the fin and on the wing at the wing-fin junction were coincident. The arrangement of the doublet-lattice boxes is shown in figure 5.

In addition to the doublet-lattice calculations made by using NASTRAN, flutter calculations for the basic wing were made by using subsonic kernel-function unsteady lifting surface theory. The technique used to generate the kernel-function unsteady aerodynamic forces was based on that in reference 9.

Thirty-six collocation points were used. The modal data used for the kernel-function analysis were the same as that used for the doublet-lattice calculations. The kernel-function flutter results were obtained by using the system of computer programs described in reference 10.

RESULTS AND DISCUSSION

The basic-wing configuration was tested in a nonlifting condition ($\alpha = 0^\circ$) and in three lifting conditions ($\alpha = 2^\circ$, 3°, and 4°). The wing-with-fin configuration was tested at $\alpha = 0^\circ$ and $\alpha = 4^\circ$. The flutter characteristics of each configuration are presented and discussed in this section. The effects of angle of attack on the flutter characteristics are described. The experimental results for each configuration in the nonlifting condition are correlated with analytical results, and, finally, the flutter results for the two configurations are compared.

Basic-Wing Configuration

The experimental results for the basic wing at angles of attack α of 0°, 2°, 3°, and 4° are presented in table I and figure 6. The data presented in the figure are the variations with Mach number of the square root of the mass-ratio parameter μ, of the flutter-frequency ratio f_f/f_2, and of the flutter-speed index parameter V_I. The flutter-speed index parameter curves represent stability boundaries, with the stable region (no flutter) below the curve. This parameter depends on the physical properties of the model, in particular the stiffness, and the atmosphere in which it operates. When plotted as a function of Mach number, curves of constant dynamic pressure are lines parallel to the Mach number abscissa. The mass-ratio parameter μ is defined as the ratio of the mass of the model to a mass of a representative surrounding volume of test medium. The volume of 0.0271 m^3 (0.956 ft^3) used in this study is that contained in the conical frustrum generated by rotating the trapezoidal planform indicated by the dashed lines in figure 1 in pitch about its midchord. (Although it is customary to use the volume circumscribed by rotating the entire model in pitch about its midchord, this was not done because it is believed the volume thus produced is weighted too heavily by the relatively large root section and, therefore, too large.) The measured frequency of the second natural mode f_2 was used as the reference frequency. The reference length b_r used was the semichord at the three-quarter span. This length is 0.0972 m (0.319 ft).

No unusual trends are shown by the data presented in figure 6. The flutter boundary for $\alpha = 0^\circ$ (fig. 6(a)) is similar to that usually observed, namely, as Mach number increases the flutter-speed index gradually decreases to a minimum value at transonic speeds and then increases as the flow becomes supersonic. The minimum flutter speed occurred at about Mach number 0.95. The flutter speed at this Mach number was about 89 percent of the value at $M = 0.70$. The flutter boundaries for $\alpha = 2^\circ$, 3°, and 4° shown in figures 6(b), 6(c), and 6(d), respectively, are similar to the $\alpha = 0^\circ$ results, although sufficient data were not obtained in all cases to define the transonic minimum.

A careful comparison of the flutter boundaries in figure 6 shows that the flutter speed decreases slightly with increasing angle of attack. This effect can be seen better in figure 7 where the flutter results are presented as the variations of flutter frequency and dynamic pressure with Mach number. From the results in figure 7 it is clear that increasing angle of attack has a destabilizing effect on the flutter dynamic pressure. The effect, however, is relatively small. The largest reduction was about 13 pecent which occurred near $M = 0.9$ for $\alpha = 4^{\circ}$. (The suppressed zero of the dynamic pressure ordinate in figure 7 tends to magnify the differences.) The flutter frequencies are affected to a small degree by angle of attack, but the effect is not as systematic as the effect on dynamic pressure. Although the reason for the reduction in flutter speed is not known, it may be due to an increase in lift-curve slope produced by vortex flow. An increase in lift-curve slope usually has the effect of reducing flutter speed. It is well known that highly swept, sharp-leading-edge wings exhibit vortex flow at very small angles of attack.

A comparison of calculated and experimental results for the basic wing is presented in figure 8 as the variations with Mach number of flutter frequency and dynamic pressure. The experimental data are the faired curves for $\alpha = 0^{\circ}$ from figure 7. The doublet-lattice calculated data are in reasonably good agreement with the experimental results both in terms of magnitude and Mach number trend. The magnitude of the kernel-function results do not agree as well with the experimental data, but the kernel-function results do exhibit the proper Mach number trend. At $M = 0.8$, for example, the flutter dynamic pressure obtained by using doublet-lattice aerodynamic forces is only about 4 percent lower than the experimental value whereas the kernel-function dynamic pressure is about 18 percent lower.

Wing-With-Fin Configuration

The experimental results for the wing-with-fin configuration at angles of attack of 0° and 4° are presented in table II and figure 9. The format of the data is the same as discussed previously for the basic-wing configuration. Although not enough data were obtained to define the minimum transonic flutter velocity, the results do show the usual decrease in flutter velocity with increasing subsonic Mach number.

A comparison of the $\alpha = 0^{\circ}$ boundary (fig. 9(a)) with $\alpha = 4^{\circ}$ (fig. 9(b)) shows that the flutter speed is slightly lower for the lifting case. The effect is seen better by comparing the flutter boundaries in terms of dynamic pressure as presented in figure 10. The flutter dynamic pressure for the lifting case ($\alpha = 4^{\circ}$) is lower throughout the Mach number range. The difference generally increases as subsonic Mach number increases. The maximum difference occurs near $M = 0.95$ where the reduction is about 13 percent of the nonlifting value ($\alpha = 0^{\circ}$) or about the same difference observed for the basic wing (fig. 8).

A comparison of calculated and experimental results for the wing-with-fin configuration are presented in figure 11 as the variation with Mach number of flutter frequency and dynamic pressure. The experimental curve shown is the faired curve for $\alpha = 0^{\circ}$ from figure 10. The calculated results agree fairly well with the experimental data although the calculated results show less of

a decrease in flutter dynamic pressure with increasing Mach number than was found experimentally. The calculated data shown in figure 11 were obtained with both structural and aerodynamic effects of the fin included.

Comparison of Basic-Wing and Wing-With-Fin Configurations

The addition of the fin to the basic wing resulted in a substantial increase in the flutter dynamic pressure. This effect can be seen by comparing the flutter results shown in figure 12. The curves shown in figure 12 are the faired curves for $\alpha = 0^{\circ}$ from figure 7 (basic wing) and figure 10 (wing-with-fin). The flutter dynamic pressure for the wing-with-fin is higher throughout the Mach number range. At $M = 0.80$, for example, the dynamic pressure is about 20 percent higher. This difference could be caused by structural effects (mass and stiffness) and/or aerodynamic effects resulting from the addition of the fin to the basic wing. To determine whether the effects were structural or aerodynamic, some additional calculations were made for $M = 0.80$ with only structural effects of the fin included - the fin was not allowed to produce aerodynamic forces. The results of this analysis are within 1 percent of those obtained with both structural and aerodynamic effects included (fig. 11). It is concluded, therefore, that the effects on flutter of adding the fin are due primarily to structural changes.

CONCLUSIONS

Experimental transonic flutter boundaries of a simplified 1/50-size, aspect-ratio-1.77 arrow-wing model have been presented for the model in a non-lifting condition (angle of attack $\alpha = 0^{\circ}$) and in three lifting conditions ($\alpha = 2^{\circ}, 3^{\circ}, 4^{\circ}$). Experimental boundaries for $\alpha = 0^{\circ}$ and 4° have been presented also for the basic wing model with a ~~ventral~~ VERTICAL fin attached at the 0.694 semispan station.

The following conclusions can be drawn from this study:

(1) The flutter characteristics of the basic-wing and wing-with-fin configurations were similar to those usually observed.

(2) Increasing angle of attack (increasing lift) reduced the flutter dynamic pressure. This effect was small (about 13 percent maximum for $\alpha = 4^{\circ}$) and was similar for both configurations.

(3) The addition of the fin to the basic wing resulted in an increase in flutter dynamic pressure. Analytical results indicated that this increase was due to structural effects (mass and stiffness) rather than aerodynamic effects.

(4) Calculated subsonic flutter results for both configurations obtained by using doublet-lattice unsteady aerodynamic theory correlate reasonably well with experimental results. Calculated flutter results for the basic wing obtained by using subsonic kernel-function unsteady aerodynamic theory did not agree as well with the experimental data.

Langley Research Center
National Aeronautics and Space Administration
Hampton, VA 23665
December 4, 1980

REFERENCES

1. Turner, M. J.; and Bartley, J. B.: Flutter Prevention in Design of the SST. Dynamic Response of Structures, George Herrmann and Nicholas Perrone, eds., Pergamon Press, Inc., c.1972, pp. 95-112.

2. Robinson, James C.; Yates, E. Carson, Jr.; Turner, M. Jonathan; and Grande, Donald L.: Application of an Advanced Computerized Structural Design System to an Arrow-Wing Supersonic Cruise Aircraft. AIAA Paper No. 75-1038, Aug. 1975.

3. Sakata, I. F.; and Davis, G. W.: Arrow-Wing Supersonic Cruise Aircraft Structural Design Concepts Evaluation. Volume 2. NASA CR-132575-2, 1976.

4. Sobieszczanski-Sobieski, J.; Gross, David; Kurtze, William; Newsom, Jerry; Wrenn, Gregory; and Greene, William. Supersonic Cruise Research Aircraft Structural Studies: Methods and Results. Supersonic Cruise Research '79 - Part 2, NASA CP-2108, 1980, pp. 617-656.

5. Doggett, Robert V., Jr.; and Ricketts, Rodney H.: Some Experimental and Theoretical Flutter Characteristics of an Arrow-Wing Configuration. Volume B - Dynamics Structural Dynamics, AIAA/ASME 18th Structures, Structural Dynamics & Materials Conference, Mar. 1977, pp. 127-132. (Available as AIAA Paper 77-422.)

6. The NASTRAN Theoretical Manual (Level 16.0). NASA SP-221(03), 1976.

7. The NASTRAN User's Manual (Level 16.0). NASA SP-222(03), 1976.

8. Rodden, William P.; Harder, Robert L.; and Bellinger, E. Dean: Aeroelastic Addition to NASTRAN. NASA CR-3094, 1979.

9. Watkins, Charles E.; Woolston, Donald S.; and Cunningham, Herbert J.: A Systematic Kernel Function Procedure for Determining Aerodynamic Forces on Oscillating or Steady Finite Wings at Subsonic Speeds. NASA TR R-48, 1959.

10. Desmarais, Robert N.; and Bennett, Robert M.: User's Guide for a Modular Flutter Analysis Software System (FAST Version 1.0). NASA TM-78720, 1978.

TABLE I.- BASIC-WING CONFIGURATION EXPERIMENTAL FLUTTER RESULTS

[b_r = 0.0972 m (0.319 ft); f_2 = 45.5 Hz; m = 6.68 kg (3.03 lbm); v = 0.0271 m^3 (0.956 ft^3); ω_2 = 285.88 rad/sec]

M	α, deg	V		ρ		q		μ	$\sqrt{\mu}$	V_I	f_f, Hz	f_f/f_2
		m/sec	ft/sec	kg/m^3	$slug/ft^3$	kPa	lbf/ft^2					
(a) α = 0°												
0.720	0.0	111.9	367.2	1.975	0.003831	12.4	258.3	25.71	5.07	0.794	34.0	0.747
.733	0.0	113.9	373.8	1.888	.003664	12.3	256.0	26.89	5.19	.790	34.0	.747
.800	0.0	124.4	408.0	1.534	.002976	11.9	247.7	33.11	5.75	.778	32.0	.703
.809	0.0	125.8	412.6	1.526	.002961	12.1	252.0	33.28	5.77	.784	31.6	.695
.850	0.0	132.1	433.5	1.294	.002512	11.3	236.0	39.23	6.26	.759	29.4	.646
.888	0.0	138.0	452.9	1.186	.002301	11.3	236.0	42.81	6.54	.759	30.0	.659
.890	0.0	138.3	453.9	1.161	.002252	11.1	232.0	43.75	6.61	.753	28.3	.622
.907	0.0	141.0	462.6	1.069	.002075	10.6	222.0	47.48	6.89	.736	28.8	.633
.920	0.0	143.0	469.2	1.040	.002019	10.6	222.2	48.81	6.99	.736	28.4	.624
.933	0.0	145.0	475.8	.924	.001793	9.7	203.0	54.94	7.41	.704	26.2	.576
[a].990	0.0	153.9	504.9	.825	.001601	9.8	204.1	61.53	7.84	.706	24.7	.543
1.020	0.0	158.6	520.2	.822	.001595	10.3	215.8	61.77	7.86	.726	27.3	.600
(b) α = 2°												
0.720	2.0	111.9	367.2	1.983	0.003848	12.4	259.4	25.61	5.06	0.796	34.5	0.758
.726	2.0	112.9	370.3	1.895	.003676	12.1	252.0	26.80	5.18	.784	33.6	.738
.792	2.0	123.1	403.9	1.548	.003003	11.7	245.0	32.80	5.73	.773	32.2	.708
.800	2.0	124.4	408.0	1.527	.002963	11.8	246.6	33.25	5.77	.776	32.0	.703
.860	2.0	133.7	438.6	1.276	.002475	11.4	238.1	39.80	6.31	.762	29.9	.657
.872	2.0	135.6	444.7	1.178	.002285	10.8	226.0	43.11	6.57	.743	29.1	.640
.888	2.0	138.0	452.9	1.086	.002106	10.3	216.0	46.78	6.84	.726	28.0	.615
.900	2.0	139.9	459.0	1.056	.002049	10.3	215.8	48.09	6.93	.726	27.8	.611
.924	2.0	143.6	471.2	.928	.001801	9.6	200.0	54.70	7.40	.699	26.7	.587
1.000	2.0	155.4	510.0	.789	.001530	9.5	199.0	64.39	8.02	.697	26.3	.578
(c) α = 3°												
0.723	3.0	112.4	368.7	1.903	0.003692	12.0	251.0	26.68	5.17	0.783	33.2	0.730
.787	3.0	122.3	401.4	1.561	.003029	11.7	244.0	32.52	5.70	.772	32.0	.703
.864	3.0	134.3	440.6	1.179	.002287	10.6	222.0	43.08	6.56	.736	28.8	.633
.882	3.0	137.1	449.8	1.085	.002105	10.2	213.0	46.80	6.84	.721	28.3	.622
.922	3.0	143.3	470.2	.932	.001809	9.6	200.9	54.46	7.38	.699	27.1	.596
.940	3.0	146.1	479.4	.825	.001601	8.8	184.0	61.53	7.84	.670	25.7	.565
(d) α = 4°												
0.726	4.0	112.9	370.3	1.902	0.003691	12.1	253.0	26.69	5.17	0.786	33.2	0.730
.774	4.0	120.3	394.7	1.588	.003080	11.5	240.0	31.98	5.66	.765	32.1	.705
.858	4.0	133.4	437.6	1.217	.002361	10.8	226.0	41.74	6.46	.743	29.2	.642
.877	4.0	136.3	447.3	1.087	.002109	10.1	211.0	46.70	6.83	.718	27.7	.609
.900	4.0	139.9	459.0	.964	.001870	9.4	197.0	52.68	7.26	.693	27.0	.593
.934	4.0	145.2	476.3	.840	.001631	8.9	185.0	60.42	7.77	.672	25.8	.567

[a]Low damping

TABLE II.- ~~BASIC WING~~ Wing With Fin CONFIGURATION EXPERIMENTAL FLUTTER RESULTS

[b_r = 0.0972 m (0.319 ft); f_2 = 46.5 Hz; m = 6.715 kg (3.1072 lbm); v = 0.0271 m^3 (0.956 ft^3); ω_2 = 292.17 rad/sec]

M	α, deg	V		ρ		q		μ	$\sqrt{\mu}$	V_I	f_f, Hz	f_f/f_2
		m/sec	ft/sec	kg/m^3	$slug/ft^3$	kPa	lbf/ft^2					
(a) α = 0°												
0.746	0.0	116.0	380.5	2.229	0.004325	15.0	313.0	23.36	4.83	0.845	33.3	0.716
.863	0.0	134.2	440.1	1.490	.002891	13.4	280.0	34.95	5.91	.799	29.2	.628
.885	0.0	137.6	451.4	1.366	.002651	12.9	270.0	38.11	6.17	.784	28.0	.602
.890	0.0	138.3	453.9	1.316	.002553	12.6	263.0	39.57	6.29	.774	27.9	.600
.930	0.0	144.6	474.3	1.113	.002160	11.6	243.0	46.76	6.84	.744	26.9	.578
1.010	0.0	157.0	515.1	.886	.001719	10.9	228.0	58.78	7.67	.721	25.0	.538
(b) α = 4°												
0.875	4.0	136.0	446.3	1.341	0.002601	12.4	259.0	38.84	6.23	0.768	27.8	0.598
.900	4.0	139.9	459.0	1.155	.002240	11.3	236.0	45.09	6.72	.733	26.3	.566
.940	4.0	146.1	479.4	.942	.001827	10.1	210.0	55.28	7.44	.692	24.6	.529
.980	4.0	152.3	499.8	.842	.001633	9.8	204.0	61.85	7.86	.682	24.2	.520

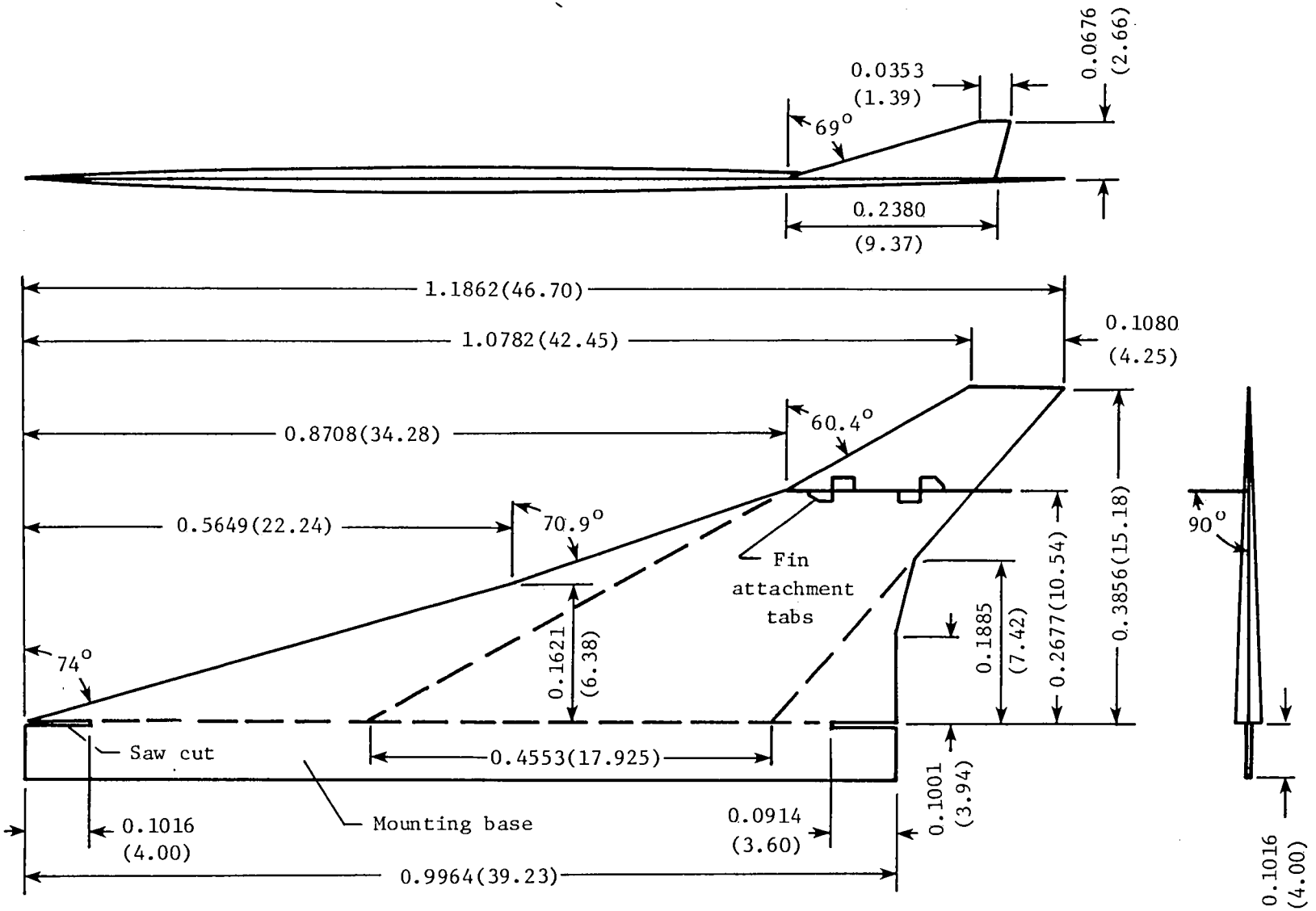

Figure 1.- Model geometry. Linear dimensions are in meters (inches).

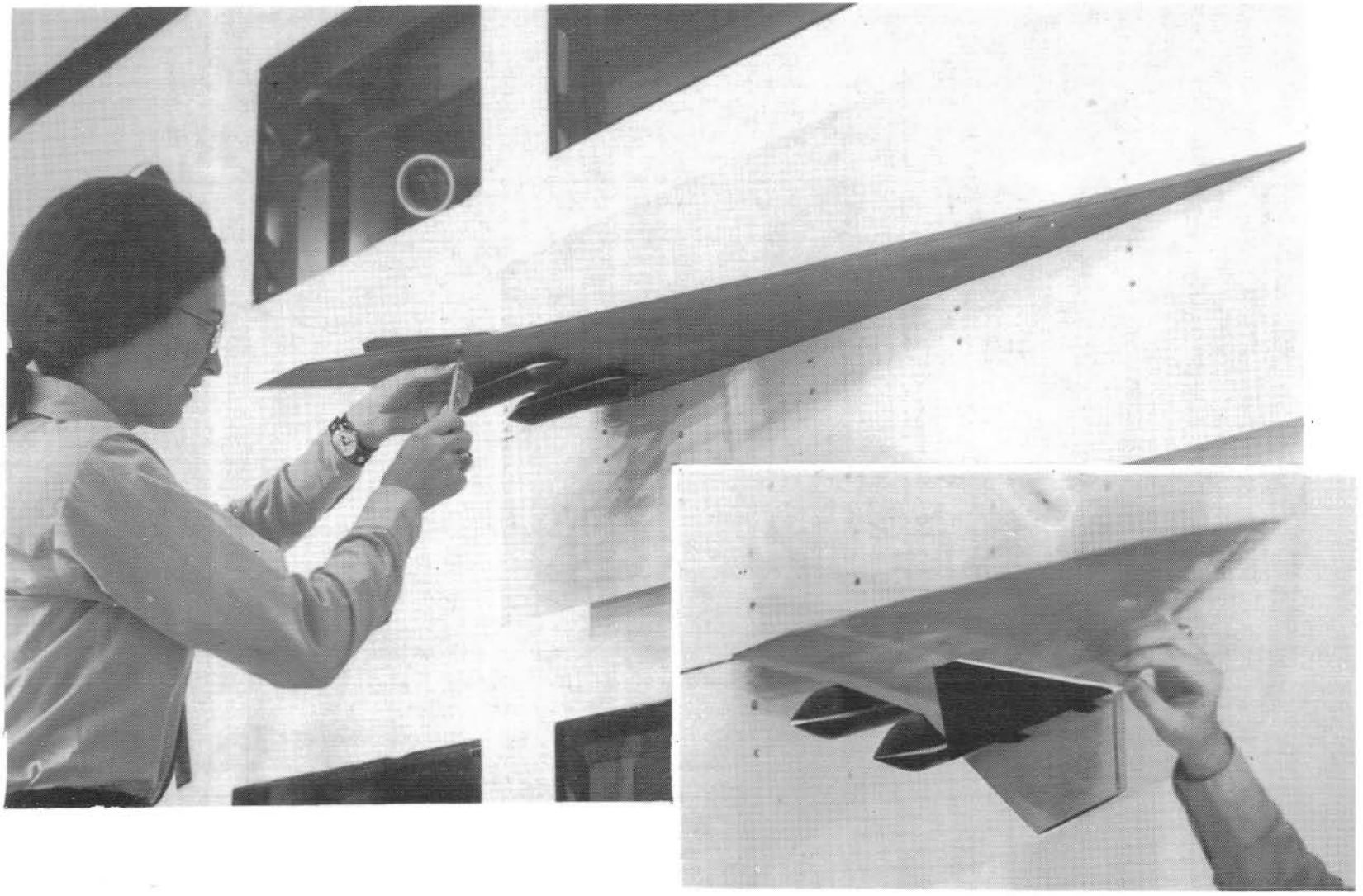

L-80-211

Figure 2.- Photographs of wing-with-fin configuration.

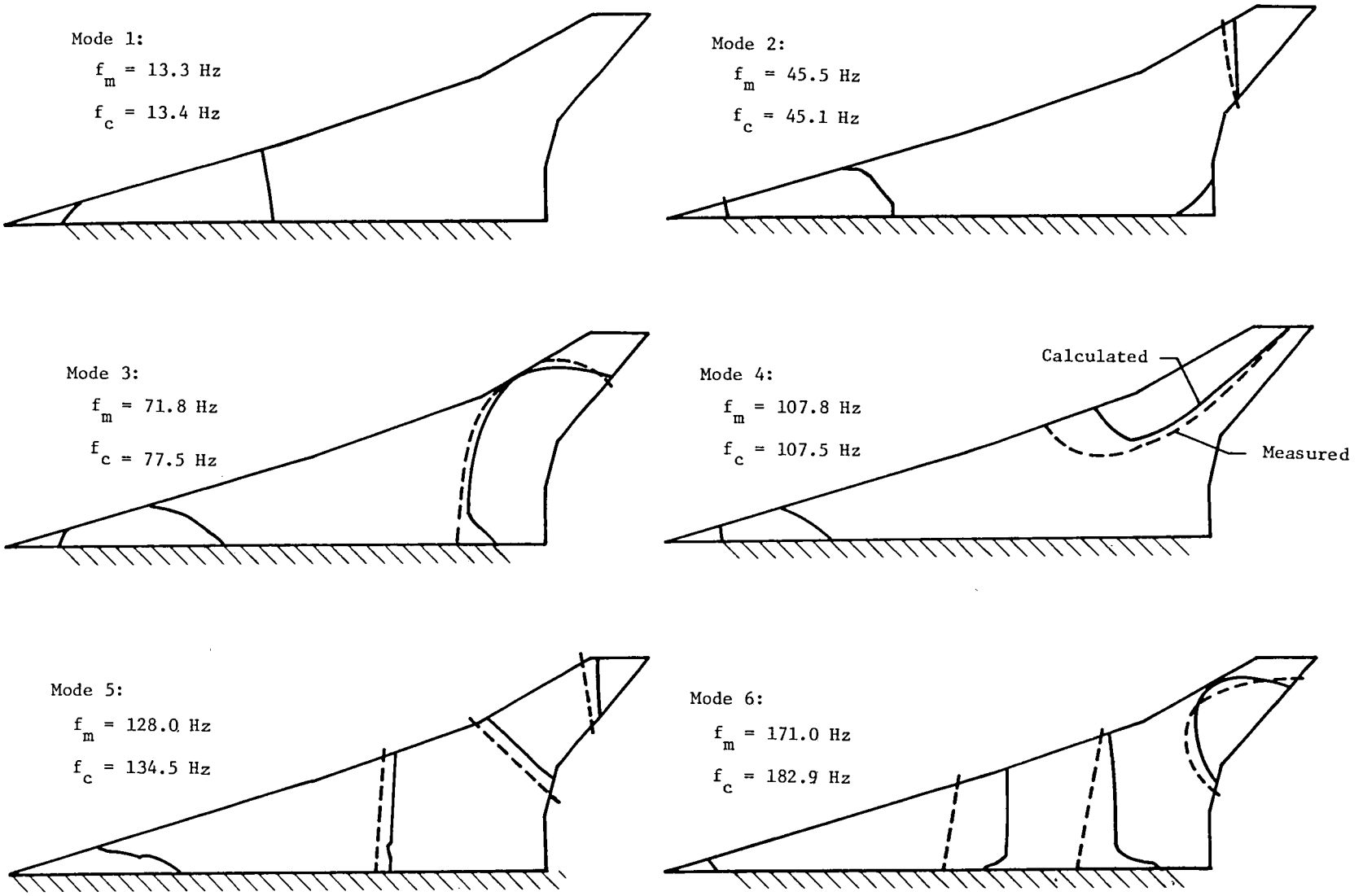

(a) Basic-wing configuration

Figure 3.- Measured and calculated natural frequencies and node lines.

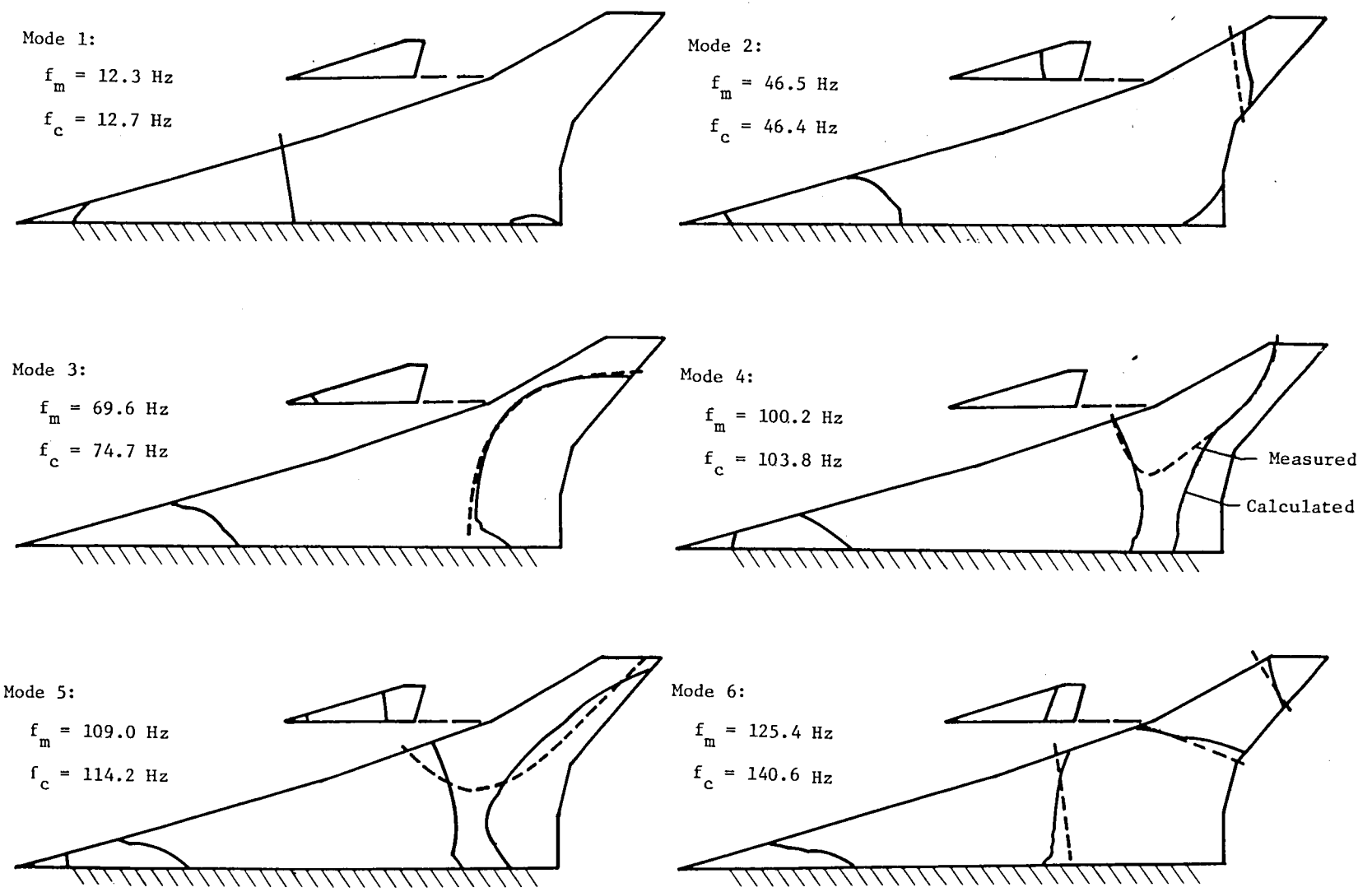

(b) Wing-with-fin configuration.

Figure 3.- Concluded.

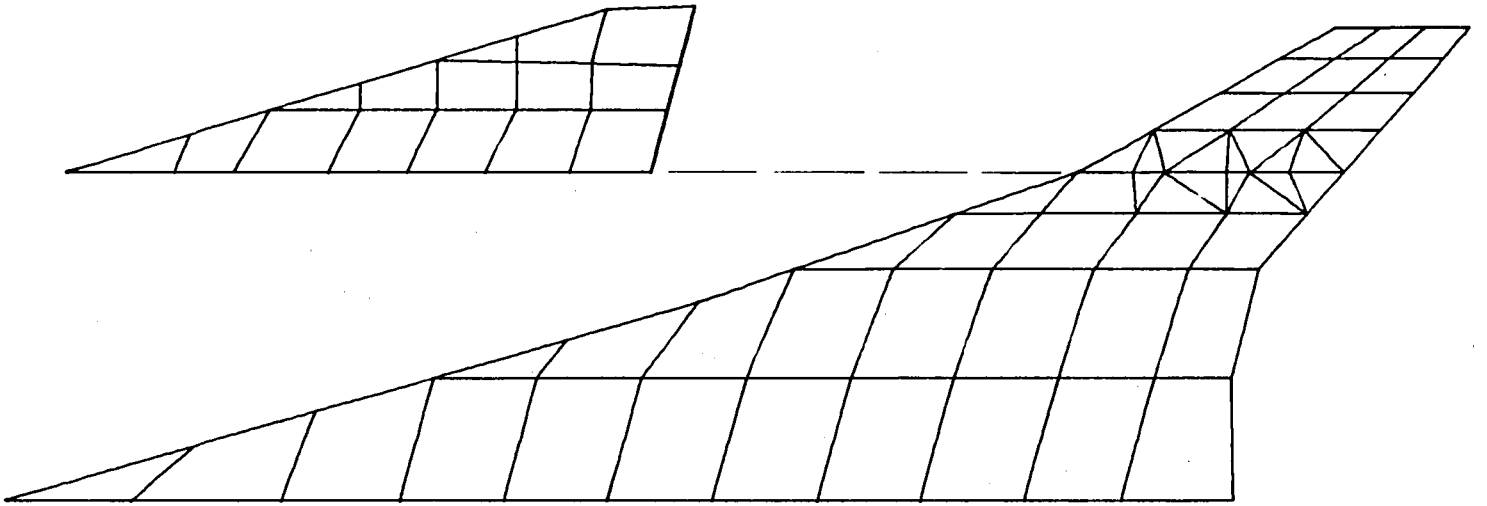

Figure 4.- Finite-element structural model. (Fin shown rotated into plane of wing and shown two times relative size.)

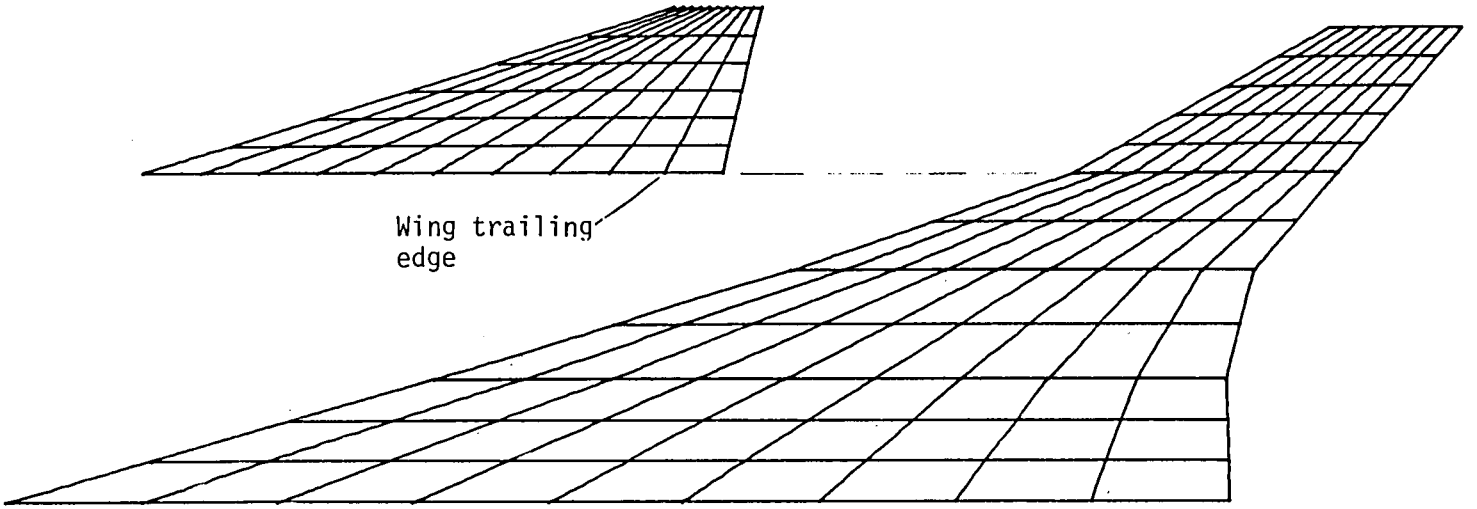

Figure 5.- Arrangement of doublet-lattice boxes. (Fin shown rotated into plane of wing and shown two times relative size.)

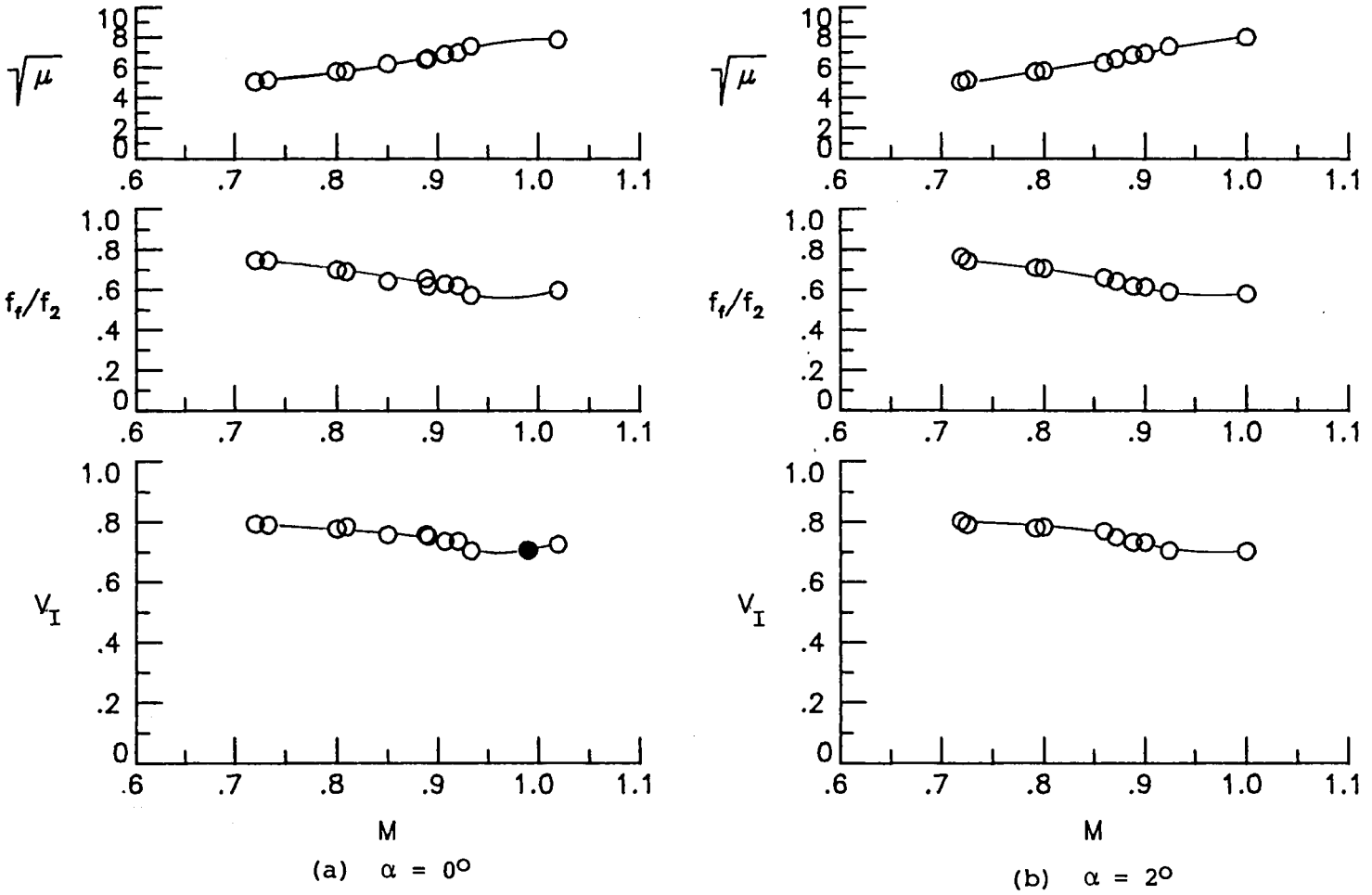

Figure 6.- Experimental flutter results for basic-wing configuration. Solid symbol indicates low damping.

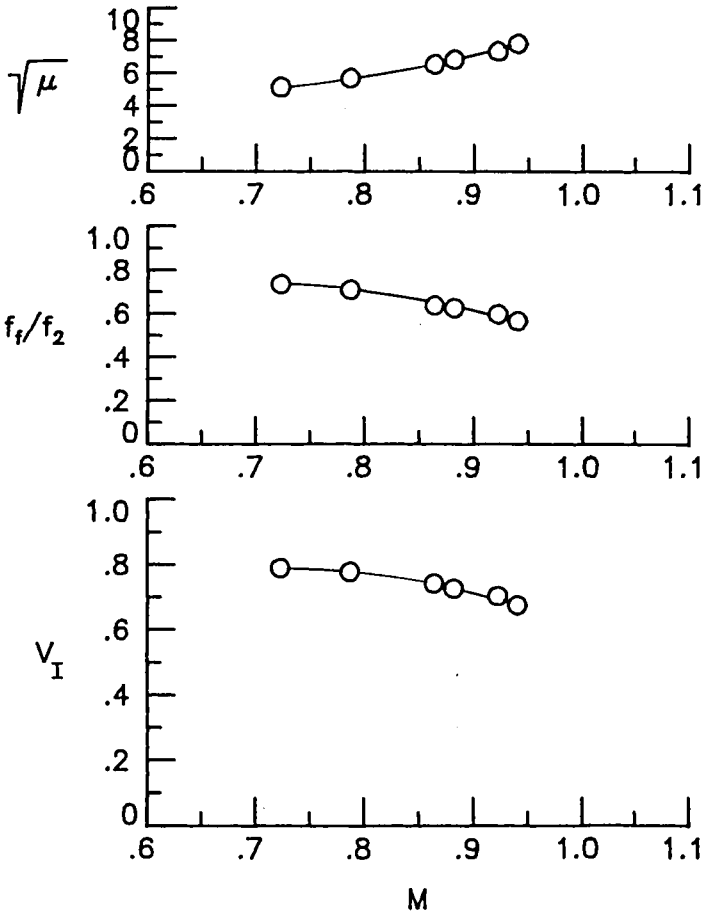

(c) $\alpha = 3^{\circ}$.

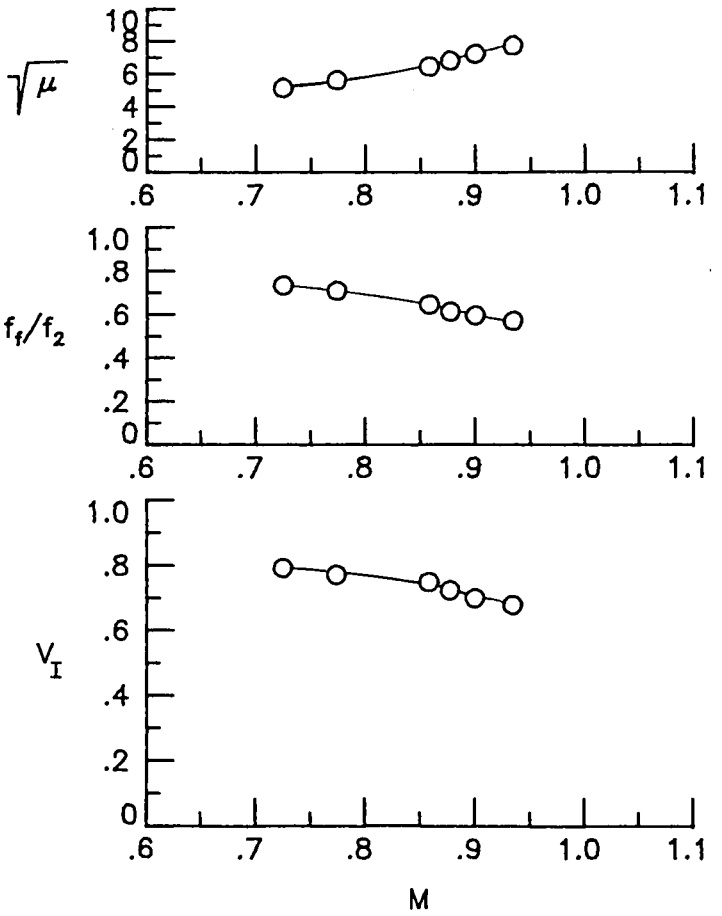

(d) $\alpha = 4^{\circ}$.

Figure 6.- Concluded.

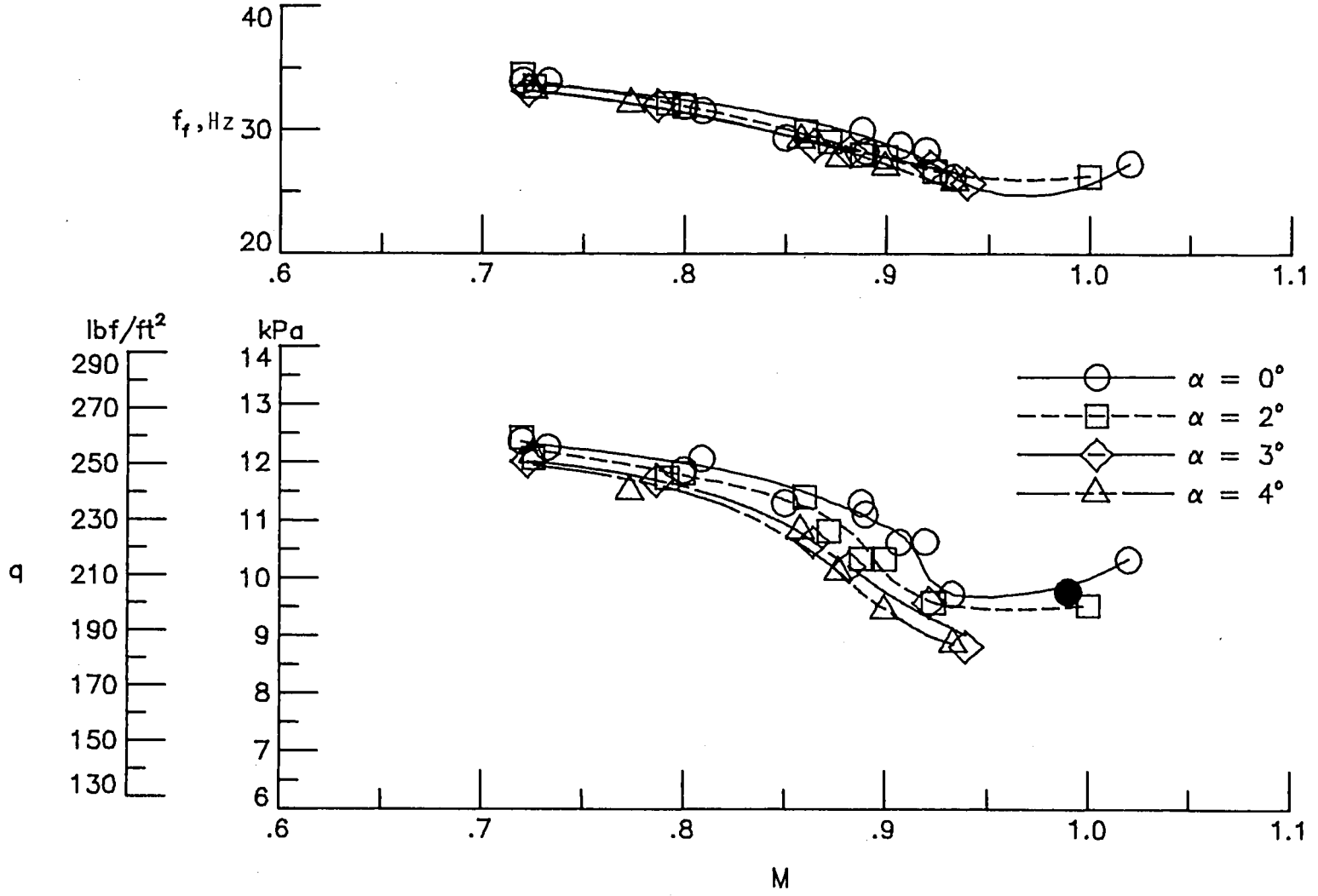

Figure 7.- Effects of angle of attack for basic-wing configuration. Solid symbol indicates low damping.

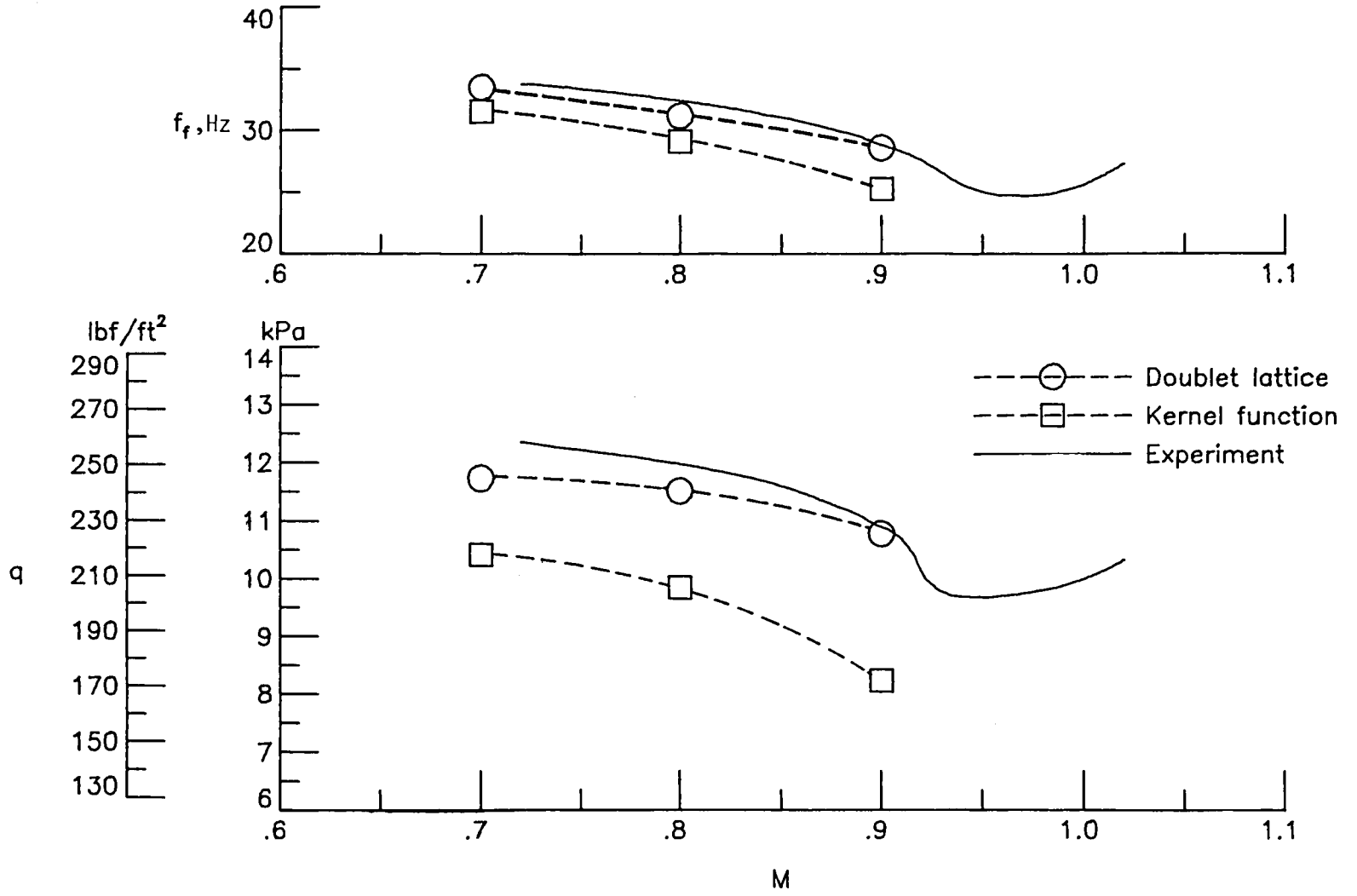

Figure 8.- Comparison of calculated and experimental flutter results for basic-wing configuration. $\alpha = 0^{o}$.

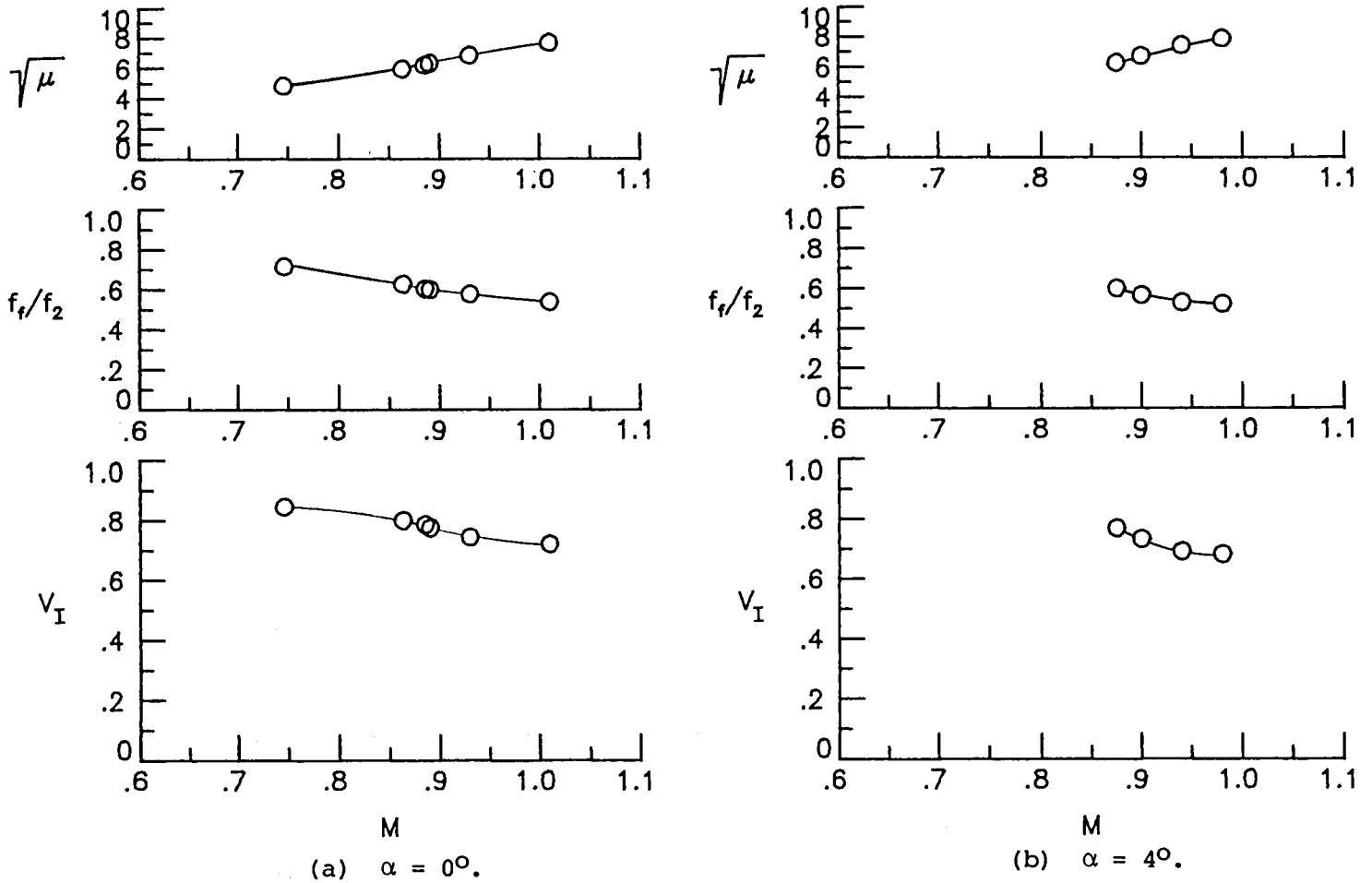

Figure 9.- Experimental flutter results for wing-with-fin configuration.

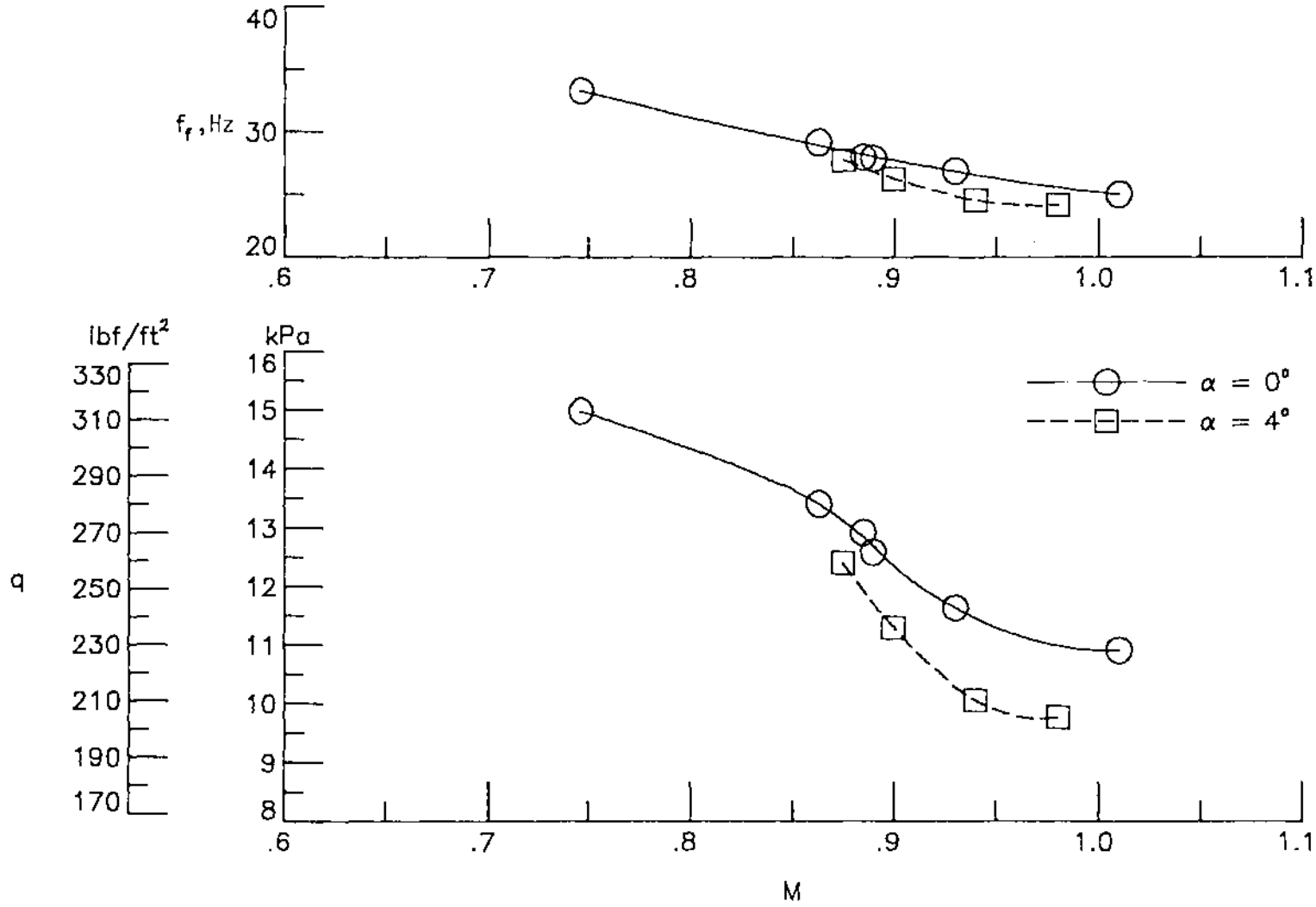

Figure 10.- Effects of angle of attack for wing-with-fin configuration.

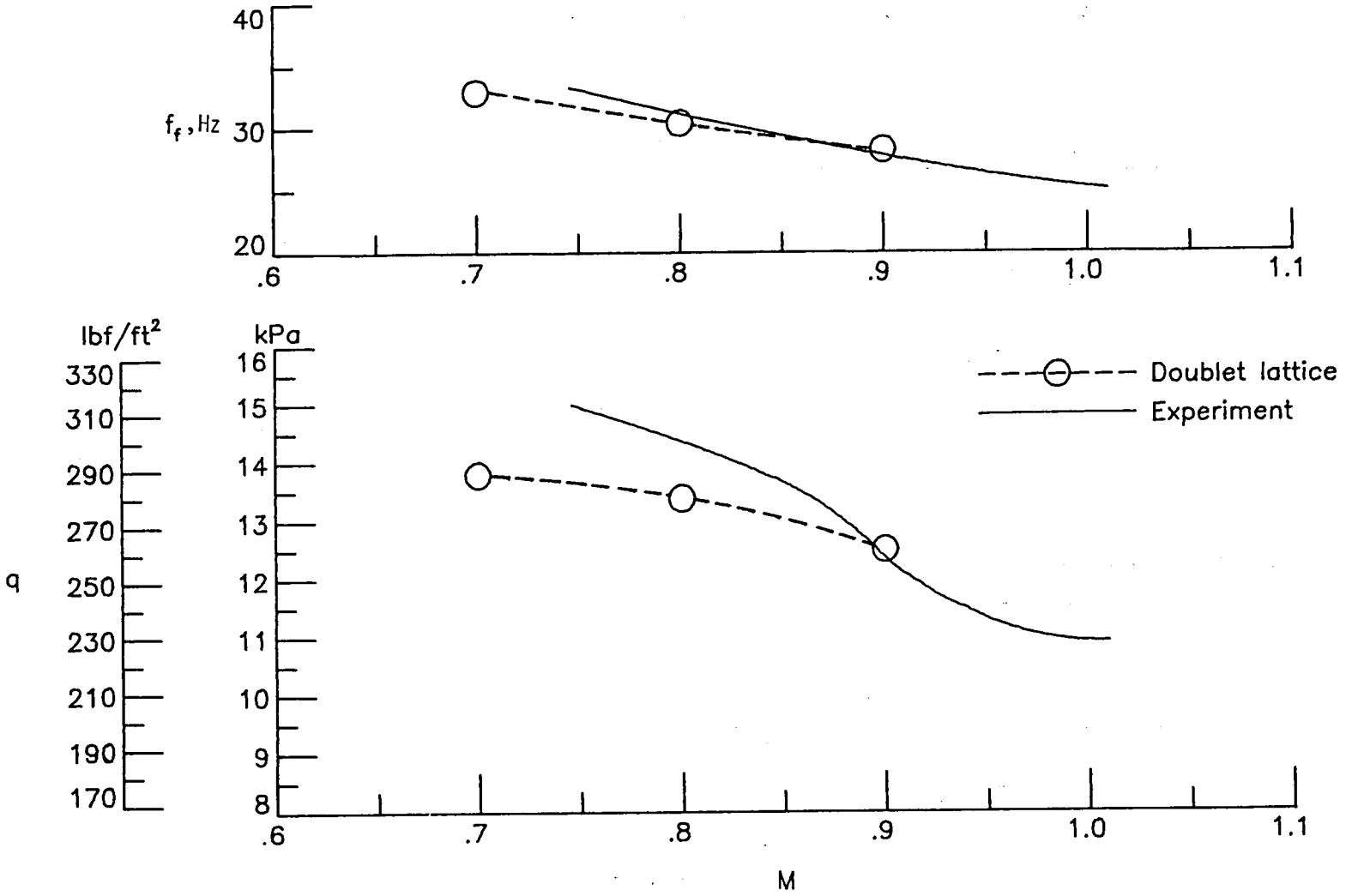

Figure 11.- Comparison of calculated and experimental flutter results for wing-with-fin configuration. $\alpha = 0^{o}$.

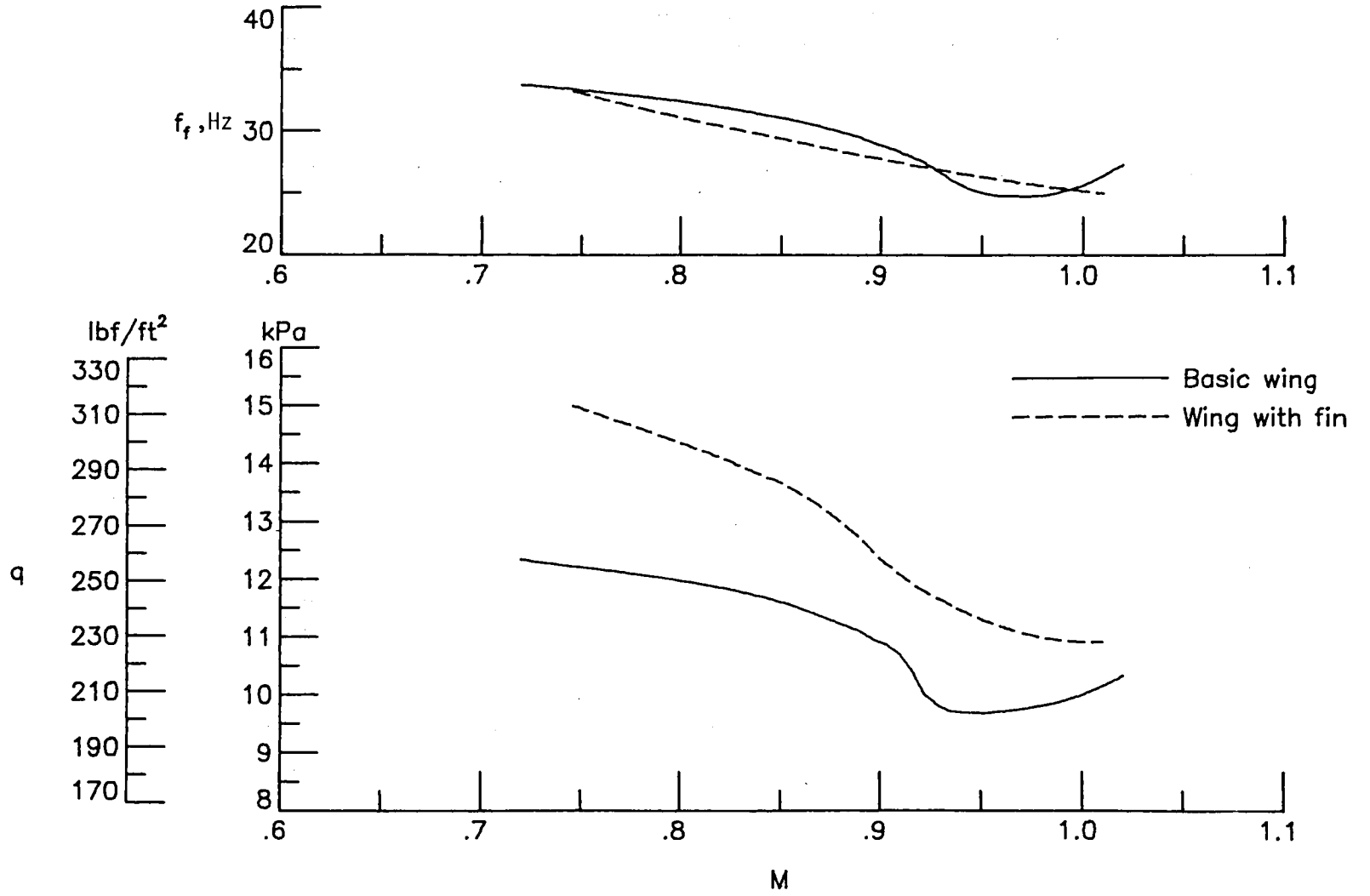

Figure 12.- Comparison of basic-wing and wing-with-fin experimental flutter results. $\alpha = 0^{o}$.

1. Report No.	2. Government Accession No.	3. Recipient's Catalog No.
NASA TM-81914		

4. Title and Subtitle	5. Report Date
EFFECTS OF ANGLE OF ATTACK AND ~~VENTRAL~~ VERTICAL FIN ON TRANSONIC FLUTTER CHARACTERISTICS OF AN ARROW-WING CONFIGURATION	December 1980
	6. Performing Organization Code 533-01-13-07
7. Author(s) Robert V. Doggett, Jr., and Rodney H. Ricketts	8. Performing Organization Report No. L-14114
	10. Work Unit No.
9. Performing Organization Name and Address NASA Langley Research Center Hampton, VA 23665	11. Contract or Grant No.
	13. Type of Report and Period Covered Technical Memorandum
12. Sponsoring Agency Name and Address National Aeronautics and Space Administration Washington, DC 20546	14. Sponsoring Agency Code

15. Supplementary Notes

16. Abstract

Experimental transonic flutter results are presented for a simplified 1/50-size, aspect-ratio-1.77 wind-tunnel model of an arrow-wing design. Flutter results are presented for two configurations; namely, one with and one without a ~~ventral~~ VERTICAL fin mounted at the 0.694 semispan station. Results are presented for both configurations trimmed to zero lift and in a lifting condition at angles of attack up to 4°. The results show that the flutter characteristics of both configurations are similar to those usually observed. Increasing angle of attack reduces the flutter dynamic pressure by a small amount (about 13 percent maximum) for both configurations. The addition of the fin to the basic wing increases the flutter dynamic pressure. Calculated results for both configurations in the nonlifting condition obtained by using subsonic doublet-lattice unsteady aerodynamic theory correlate reasonably well with the experimental results. Calculated results for the basic wing obtained by using subsonic kernel-function unsteady aerodynamic theory did not agree as well with the experimental data.

17. Key Words (Suggested by Author(s))	18. Distribution Statement
Flutter Arrow wings Angle of attack Transonic	Unclassified - Unlimited Subject Category ~~32~~ 39

19. Security Classif. (of this report)	20. Security Classif. (of this page)	21. No. of Pages	22. Price
Unclassified	Unclassified	26	A03

For sale by the National Technical Information Service, Springfield, Virginia 22161

NASA-Langley, 1980